Chinese Chemical Letters 34 (2023) 108517

Contents lists available at ScienceDirect

Chinese Chemical Letters

journal homepage: www.elsevier.com/locate/cclet

The effects of local environment towards yield and selectivity on photocatalytic CO_2 reduction catalyzed by metal-organic framework

Qianqian Huang[a,b], Rui Wang[a], Xiya Li[a], Tianfu Liu[a,b,c], A. R. Mahammed Shaheer[a,*], Rong Cao[a,b,c,*]

[a] State Key Laboratory of Structural Chemistry, Fujian Institute of Research on the Structure of Matter, Chinese Academy of Sciences, Fuzhou 350002, China
[b] University of Chinese Academy of Sciences, Beijing 100049, China
[c] Fujian Science Technology Innovation Laboratory for Optoelectronic Information of China, Fuzhou 350108, China

ARTICLE INFO

Article history:
Received 6 March 2023
Revised 20 April 2023
Accepted 26 April 2023
Available online 4 May 2023

Keywords:
Photocatalysis
CO_2
Reaction mode
Yield
Selectivity

ABSTRACT

The CO_2 photoconversion is sensitive to the local reaction environment, of which activity and selectivity can be regulated by the change of reaction systems. This paper focuses on investigating the photocatalytic CO_2 reduction behaviors of MOFs with the involvement of water under different reaction modes, including gas-solid and liquid-solid systems. The CO_2 photoreduction in a liquid-solid system shows high performance in generating HCOOH with the selectivity of 100%. In contrast, the gas-solid system referring to the synergistic interaction of MOFs and H_2O vapor benefits to the formation of gas-phase products, such as CO and CH_4. The possible mechanisms of photocatalytic CO_2 reaction in two modes were investigated by *in-situ* Fourier-transform infrared spectroscopy, which indicates that the distinction in reaction consequence may result from the difference in CO_2 chemisorbed modes and the proton provision. The choice of reaction system plays an important role in the achievement of high efficiency and selectivity for photocatalytic CO_2 reduction, which is of great practical value in real-world applications.

With the expanding scale of human production activities, the massive emission of CO_2 induced by the ever-increasing combustion of fossil fuels has caused serious environmental problems, such as global warming, environmental pollution [1]. The efficient conversion of CO_2 into valuable chemicals and fuels is consistent with the sustainable development of human society and the requirement for improved living standards [2,3]. Therefore, the exploration of CO_2 fixation has attracted extensive scientific interest in utilizing diverse strategies, including photocatalysis, electrocatalysis, biotransformation, *etc*. Among these methods, photocatalytic CO_2 reduction reaction is expected to be an advanced technology for achieving effective solar-to-chemical energy conversion [4–8]. Inorganic semiconductors have been regarded as heterogeneous photocatalysts due to their appropriate energy gap, rapid charge transfer, and high surface reaction kinetics [9,10]. However, their inherently nonporous structure renders the catalytic reactions confined to the outer surface of these materials, which results in severe e^-/h^+ pairs recombining in the bulk phase [1]. Therefore, for higher efficiency of photocatalysis, proper catalysts with excellent porosity and homo-dispersed active sites could be promising candidates for CO_2 photoconversion.

Metal-organic frameworks (MOFs) have well-defined structures, tunable pore sizes, abundant metal sites, and diverse functionalities, which determine their superiority for use in CO_2 photoreduction [11–16]. For example, NH_2-MIL-125 exhibited excellent HCOOH yield at a pressure higher than 6.89 MPa [17]. Pyrazolyl porphyrinic Ni-MOF of PCN-601 has shown good CO_2 reduction activity to produce CO and CH_4 under visible light radiation [18]. Light and catalytic environments have a significant impact on CO_2 photoconversion [19–21]. Photocatalysis in water reaction systems under visible radiation is thought to be the most efficient way to combine energy efficiency and green chemistry. In recent studies, the experiments of photo-excited CO_2 reduction catalyzed by MOFs have been observed in the liquid-solid system or in the gas-solid system [18,22]. However, thus far there has been no comparison of the photocatalytic behaviors of MOF using the two different reaction modes at the same time. Obviously, different reaction environments involved in the two catalytic modes affect the reaction kinetics and reaction pathway, resulting in different product selectivity. These results may have complex energetic and/or kinetic

* Corresponding authors at: State Key Laboratory of Structural Chemistry, Fujian Institute of Research on the Structure of Matter, Chinese Academy of Sciences, Fuzhou 350002, China.
E-mail addresses: asmshaheer@fjirsm.ac.cn (A. R. Mahammed Shaheer), rcao@fjirsm.ac.cn (R. Cao).

https://doi.org/10.1016/j.cclet.2023.108517
1001-8417/

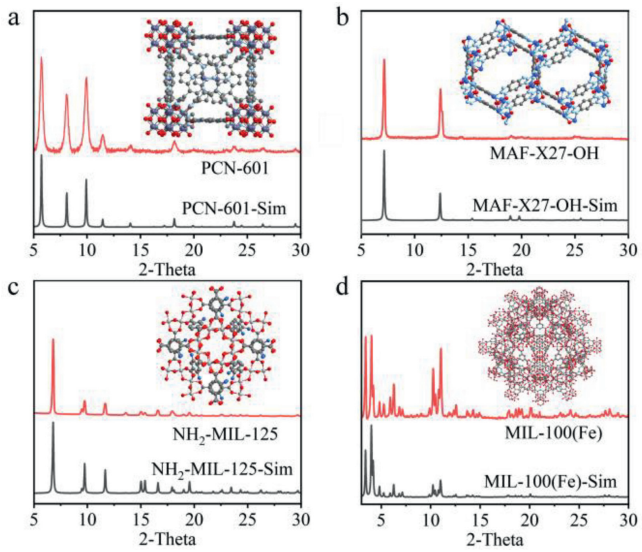

Fig. 1. The PXRD patterns and simulated structures of (a) PCN-601, (b) MAF-X27-OH, (c) NH_2-MIL-125, and (d) MIL-100(Fe).

origins, rooted in interactions among the reactants, chemical environments, and catalytic sites. Therefore, it is equally important to explore the effect of the reaction system on the product selectivity of photocatalytic CO_2 reduction as well as to develop efficient photocatalysts.

In this article, we discuss the effect of local environment systems on the activity and selectivity of photocatalytic CO_2 reduction catalyzed by MOF. Four different MOFs of PCN-601, NH_2-MIL-125, MAF-X27-OH, and MIL-100(Fe) were selected as photocatalysts and pure H_2O in the chemical system was used as sacrificial electron and proton donor. Under the visible light radiation and CO_2 atmosphere, the catalyst was placed above or below the water surface to create a gas-solid or liquid-solid system for CO_2 conversion. We found that the direct contact of the catalyst with liquid H_2O contributes to the formation of HCOOH with the selectivity of 100%, and the synergistic interaction of MOFs and H_2O vapor in a gas-solid system is in favor of the formation of gas-phase products, such as CO and CH_4. The difference in reaction results may be caused by the difference in CO_2 bridging mode and proton concentration. These observations provide insights into how changes in the local chemical environment affect the yield and selectivity of catalysts and improve the reference for the design of CO_2 reduction systems.

The selection of inorganic metal clusters and organic linkers is a key step in the design and synthesis of MOF photocatalysts. Fig. 1 shows the structures of MOFs assembled by several types of metal clusters and organic linkers. According to the clear structure of PCN-601 framework ($Ni_8(OH)_4(H_2O)_2TPP_3$), the ligands of PCN-601 (H_4TPP = 5,10,15,20-tetra(1*H*-pyrazol-4-yl)porphyrin) have a larger π-conjugated system and a higher π-d orbital overlap with the Ni-oxo nodes, beneficial to the transfer of electrons from the ligand to the metal node, which suppresses the carriers recombination and provides sufficient electrons for the reduction reaction at the metal sites [18]. MAF-X27-OH ($Co_2(\mu\text{-}OH)_2$(bbta), H_2bbta = 1*H*,5*H*-benzo(1,2-*d*:4,5-*d*')bistriazole) is obtained by ion exchange of MAF-X27-Cl, in which the μ-OH^- ligands act as Brönsted acid-type functional group cooperating with the adjacent metal centers [23]. The μ-OH^- ligands not only can act as hydrogen bond donors to stabilize CO_2, but they can also provide protons to promote the cleavage of C-O bonds of CO_2. NH_2-MIL-125 ($Ti_8O_8(OH)_4$(bdc-NH_2)$_6$, bdc-NH_2 = 2-amino-benzene-1,4-dicarboxylate) has excellent photochemical stability. The -NH_2 functional group embedded in the benzene moieties can improve the interaction with CO_2 molecules as well as broaden the optical response range, and the Ti^{IV}/Ti^{III} ion pairs on the metal nodes can facilitate the local charge transfer, which is conducive to the CO_2 photoconversion [24]. MIL-100(Fe) ($Fe^{III}_3O(H_2O)_2F\cdot\{C_6H_3(CO_2)_3\}_2\cdot nH_2O$ (n~14.5)) is constructed with uniform Fe-oxo clusters, and four μ_3-O bridged Fe_3O clusters together form a tetrahedron as a building unit [25]. The compact structural unit arrangement of MIL-100(Fe) facilitates electron migration for driving CO_2 reduction [26]. The above-mentioned four MOFs with well-defined structures were synthesized by conventional solvothermal or hydrothermal methods followed by activated procedure. The X-ray diffraction (XRD) patterns of activated samples and simulated MOFs are shown in Fig. 1. The sharp diffraction peaks of all samples are in good agreement with those of the simulated XRD structures, indicating that the obtained samples with high crystallinity have the desired construction.

Table 1
Bandgap, CB/VB position and absorption edge of the prepared MOF.

Sample	PCN-601	MAF-X27-OH	NH_2-MIL-125	MIL-100(Fe)
E_g (eV)	1.77	1.90	2.44	2.55
CB/VB (V)	−0.68/1.09	−0.76/1.14	−0.78/1.66	−0.91/1.64
Absorption edge (λ, nm)	701	653	506	485

The morphologies of the as-synthesized MOFs were observed *via* scanning electron microscopy (SEM). As shown in Figs. 2a–d, the as-synthesized MOFs show their morphologies as nano-sized crystals, among which the particle size distributions of PCN-601 is around 50–100 nm. Likewise, NH_2-MIL-125 and MIL-100(Fe) are nanoscale blocks with relatively larger size about 100–1000 nm. By contrast, MAF-X27-OH is columnar crystal reaching a length of micron level. For further measurement of the porous structures, N_2 adsorption experiments of all as-synthesized MOFs were conducted at the temperature of 77 K. The measured N_2 adsorption-desorption isotherms and calculated Brunauer-Emmett-Teller (BET) specific surface area are displayed in Figs. 2e–h. As-synthesized MOFs all showed typical type I adsorption isotherms, indicating the microporous nature. The BET surface areas of PCN-601, MAF-X27-OH, NH_2-MIL-125, and MIL-100(Fe) were 1034, 923, 1479 and 2029 m^2/g, respectively. In addition, the pore size distributions of the four MOF samples obtained from the N_2 sorption results (5.9 and 6.6 Å, 6.0 and 7.2 Å, 6.3 and 8.8 Å, 11.9 and 18.7 Å for PCN-601, MAF-X27-OH, NH_2-MIL-125, and MIL-100(Fe), respectively) are large enough for the mass transport of H_2O molecules ($3.71\times3.12\times2.86$ Å^3) and CO_2 molecules ($3.20\times3.20\times7.90$ Å^3) (Figs. S1 and S2 in Supporting information). This means that the pore surfaces of all MOFs are accessible to catalytic reactants.

The UV–vis spectra were used to evaluate the light harvesting properties of the catalysts. As shown in Fig. 3, all the as-synthesized MOFs can respond to a proper visible light range, suggesting their potential for catalytic reactions under visible light radiation. From the Tauc plot, the bandgaps of PCN-601, MAF-X27-OH, NH_2-MIL-125, and MIL-100(Fe) were estimated to be 1.77, 1.90, 2.44 and 2.55 eV *via* K-M transformation, respectively (Fig. S3 in Supporting information). Moreover, Mott-Schottky measurements were determined at a frequency of 1000, 1200 and 1500 Hz as shown in Fig. S4 (Supporting information) [27]. The results indicate that the synthesized MOFs are all n-type semiconductors. And the measured conduction band (CB) positions of PCN-601, MAF-X27-OH, NH_2-MIL-125 and MIL-100(Fe) are estimated to be −0.68, −076, −0.78 and −0.91 V *vs.* NHE, respectively. The valence band (VB) of all four MOFs can be calculated to be 1.09, 1.14, 1.66 and 1.64 V *vs.* NHE, respectively. Because their CB position is relatively negative, it is theoretically feasible for these MOFs to be used as catalysts for the photoreduction of CO_2 (Table 1).

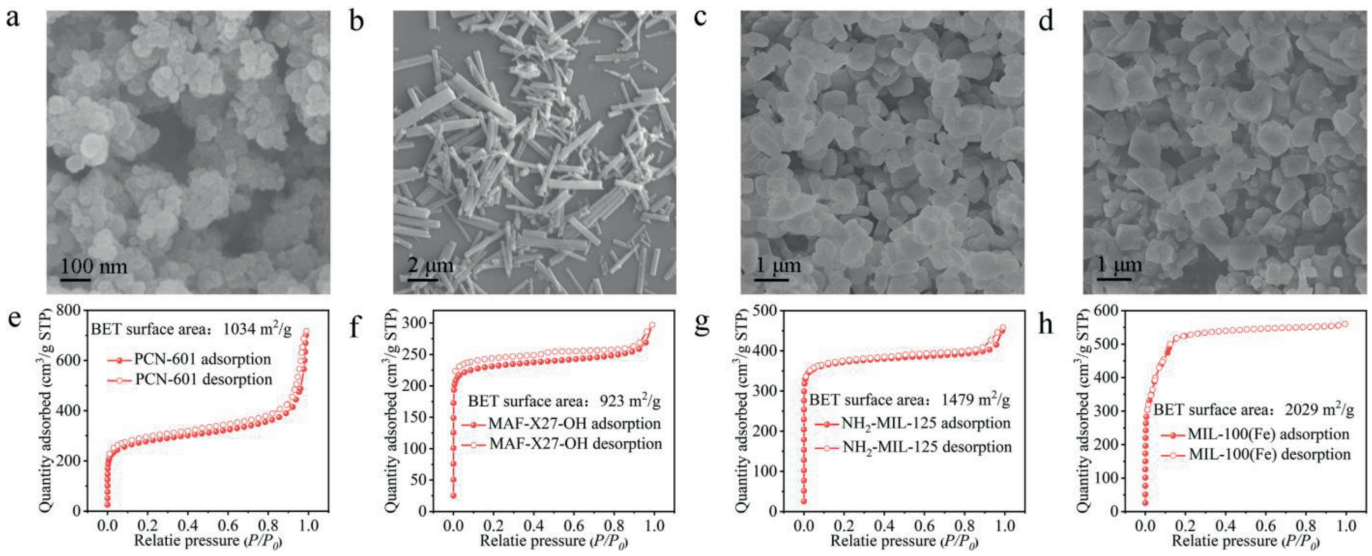

Fig. 2. SEM images and N_2 adsorption-desorption isotherms of (a, e) PCN-601, (b, f) MAF-X27-OH, (c, g) NH_2-MIL-125, and (d, h) MIL-100(Fe).

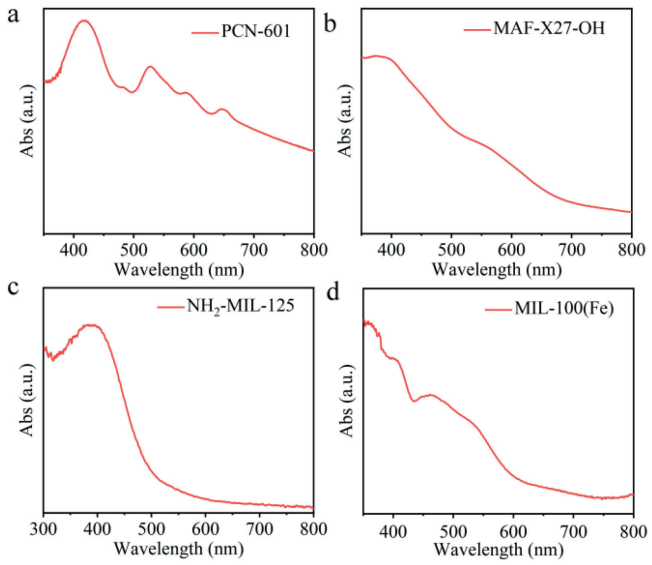

Fig. 3. The UV–vis spectra of samples. (a) PCN-601, (b) MAF-X27-OH, (c) NH_2-MIL-125, and (d) MIL-100(Fe).

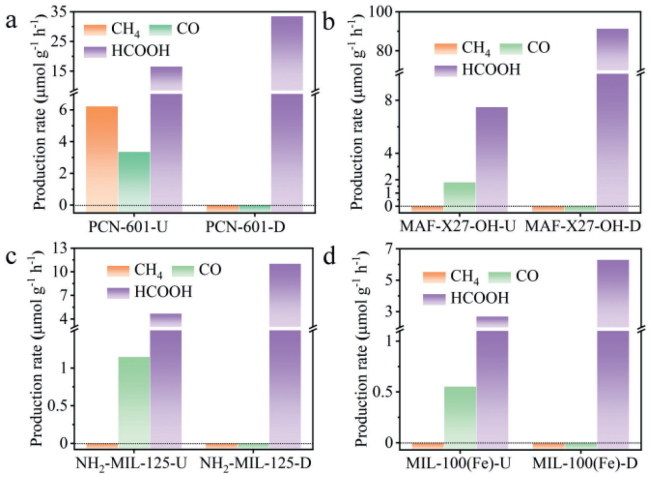

Fig. 4. Photocatalytic CO_2 reduction activity of as-synthesized MOFs with visible radiation under different reaction systems. (a) PCN-601, (b) MAF-X27-OH, (c) NH_2-MIL-125, and (d) MIL-100(Fe).

Based on the above analysis and characterization, the selected MOFs have the potential to be utilized in the photocatalytic CO_2 reduction experiment. Meanwhile, to further reveal the specific effects of the chemical environment on the catalytic reaction, two typical photocatalytic reaction systems of gas-solid and liquid-solid modes were established under visible light radiation in a water environment and a pure CO_2 (80 kPa, 288 K) atmosphere (Figs. S5 and S6 in Supporting information). The powder catalyst was fixed on a quartz filter, and then the filter slices were placed above or below the water surface (denoted as U or D), representing gas-solid and liquid-solid systems, respectively. As shown in Fig. 4 and Fig. S7 (Supporting information), the gas-solid photocatalytic reactions mainly generate HCOOH, CO, and CH_4 products after 10 h of illumination, and their generation rates are presented in Table 2. In the gas-solid systems, HCOOH is the main product of CO_2 reduction (16.6 μmol g^{-1} h^{-1} for PCN-601, 7.50 μmol g^{-1} h^{-1} for MAF-X27-OH, 4.70 μmol g^{-1} h^{-1} for NH_2-MIL-125, and 2.70 μmol g^{-1} h^{-1} for MIL-100(Fe)), but the corresponding production selectivity of HCOOH is relatively low (63.4% for PCN-601, 80.5% for MAF-X27-OH, 80.3% for NH_2-MIL-125, and 80% for MIL-100(Fe)). Among these, only PCN-601 exhibits obvious activity for generating CH_4, which has been demonstrated in the previous study [12]. In sharp contrast, liquid-solid systems show a markedly different

Table 2
Effect of reaction system on catalytic behaviors of different MOFs.

Catalyst	Reaction system	Production rates (μmol g^{-1} h^{-1})			$Sel_{product}$ (%)[a]
		CH_4	CO	HCOOH	
PCN-601	gas-solid	6.24	3.36	16.6	63.4
	liquid-solid	0	0	33.5	100
MAF-X27-OH	gas-solid	0	1.82	7.50	80.5
	liquid-solid	0	0	91.4	100
NH_2-MIL-125	gas-solid	0	1.15	4.70	80.3
	liquid-solid	0	0	11.03	100
MIL-100(Fe)	gas-solid	0	0.55	2.70	83
	liquid-solid	0	0	6.30	100

[a] Product selectivity of HCOOH:$Sel_{product}(\%) = (v(HCOOH)/(v(CH_4) + v(CO) + v(HCOOH)) \times 100\%$, where the $v(CH_4)$, $v(CO)$ and $v(HCOOH)$ denote the production rates of CH_4, CO and HCOOH, respectively.

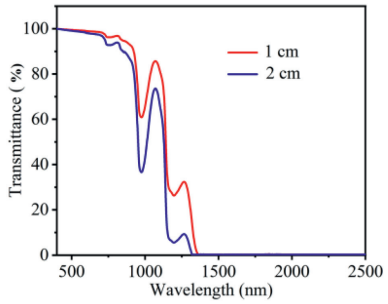

Fig. 5. Transmission spectra of light through different water thicknesses.

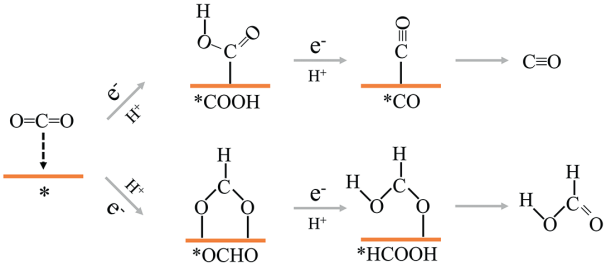

Fig. 6. Proposed reaction pathways of (a) CO and (b) HCOOH formation from CO_2.

result due to the *ca.* 100% of HCOOH selectivity catalyzed by the selected MOFs. Moreover, the rate of CO_2-to-HCOOH conversion of PCN-601, MAF-X27-OH, NH_2-MIL-125, and MIL-100(Fe) photocatalysis reached 33.5, 91.40, 11.03 and 6.30 μmol g^{-1} h^{-1}, respectively, which is significantly higher than that of the gas-solid systems. Moreover, the four tested MOFs under different reaction modes are not benefited from the particle size effect (Fig. S8 in Supporting information). It was worth pointing out that the selected MOFs perform a durability for 3 runs of cycled photocatalysis. The crystal structure of selected MOFs was well kept and a small amount of metal was leaked into solutions (liquid-solid reaction mode), indicating the good durability of selected MOFs (Figs. S9-S11 and Table S1 in Supporting information).

According to a comprehensive analysis, although the reduction of CO_2-to-HCOOH is the main reaction route of the photocatalysis of MOFs, the CO_2-to-CO/CH_4 conversion has a tendency to occur in the gas-solid systems. Considering that the diverse products could be derived from different reaction pathways, the effects of the photocatalytic modes deserve deeper exploration for explaining the different product selectivity and detailed reaction mechanism of CO_2 photoreduction.

To study the effect of H_2O on light propagation, the transmission spectra of light passing through different water layer thicknesses are shown in Fig. 5. As the water thickness increases, only the intensity of long wavelength light decays severely due to the adsorption and scattering of water ($\lambda > 710$ nm), which means that the catalyst in the liquid-solid system harvests less long wavelength visible or NIR radiation. However, the absorption edges of all selected MOFs are less than 710 nm, indicating that the difference in light irradiation in two reaction modes has no significant effect on the generation of electron/hole pairs for MOFs (Table 1). At the same time, the temperature of the reaction system was kept at 288 K, so the photothermal effect on the photocatalytic activity of MOFs can also be excluded. Consequently, light does not cause a difference in activity and selectivity in the two reaction modes.

The *in-situ* Fourier-transform infrared spectroscopy (FTIRS) collected from photochemical systems are helpful to distinguish the intermediate state of CO_2 transformation and provide key clues to understand the reaction pathway. *In-situ* FTIRS measurements were carried out for both the gas-solid and liquid-solid systems under visible radiation and kept the temperature at 288 K by circulating cooling water. As shown in Figs. S12 and S13 (Supporting information), the infrared absorption peak around 1730 cm^{-1} was obviously observed in both reaction systems, which can be attributed to C=O stretching vibration of HCOOH. In the gas-solid system, the bands centered around 1560 cm^{-1} and 1400 cm^{-1} can be assigned to the *COOH, which is a key intermediate for the conversion of CO_2 to CO [28–32]. The peaks around 1542 cm^{-1} and 1340 cm^{-1} are associated with *OCHO, supporting the CO_2 reduction to HCOOH [29,33,34]. However, in the liquid-solid system, the peaks about *COOH species are too weak to be observed, while the peaks of *OCHO are still seen. Generally, in CO_2 photoconversion, the generation of CO (−0.53 V *vs.* NHE, pH 7) and HCOOH (−0.61 V *vs.* NHE, pH 7), are considered to be driven by the multi-electron/proton transfer [35]. After the physisorption of CO_2, reactant molecules obtain one electron from photocatalysts to generate CO_2*, which is the key step in CO_2 conversion. Then, the activated species further transform into *COOH or *OCHO intermediates with the involvement of a proton (Fig. 6). In the subsequent reduction reaction, the *COOH intermediates are inclined to be converted into CO molecules with the dehydration step. By contrast, the *OCHO intermediates could be the precursor of HCOOH formation. Therefore, in the spectra of *in-situ* FTIRS, the sharper peaks of *OCHO of liquid-solid systems exhibit the higher activity of CO_2-to-HCOOH reduction, while the relatively evident peaks of *COOH of gas-solid systems demonstrate the tendency of CO_2-to-CO conversion under this condition, which is consistent with the results of photocatalytic experiments.

As mentioned above, photocatalytic CO_2 reduction involves the transfer of multiple electrons/protons [34]. Considering the difference in the local environment of the two reaction modes, we speculate that the differences in the species of products can be attributed to the proton concentration. For the reaction of a liquid-solid system, an acidic environment originated from the dissolution of CO_2 provides sufficient protons, contributing to the high efficiency of CO_2 conversion. Moreover, the products selectivity could be related to the supply of proton. As earlier mentioned, the CO_2 insertion into the active sites occurs accompanied with the addition of proton and electrons. In the liquid-solid systems, the H^- species on the photocatalyst form through a series of proton and electron transfers, and the nucleophilic H^- tends to attack the C atoms of CO_2 to generate C-H bonds, which contributes to the formation of *OCHO intermediate on the active sites with relatively low activation energy [36–46]. By contrast, the photocatalysis assisted by water vapor in the gas-solid system is in favor of the generation of gaseous products. To further verify the influence of proton concentration on photocatalytic CO_2 reduction in the gas-solid and liquid-solid systems, we add volatile acid, HCl, to the solvent (adjusting pH value to 4) for increasing the proton supply of the two reaction modes. PCN-601 can accomplish a kinetically challenging eight-electron half-reaction due to the potential of photocatalytic CO_2 reduction to CH_4. Therefore, for more intuitive verification of the change of photocatalytic product generation (CO, HCOOH, CH_4 and H_2), PCN-601 is chosen as an example to verify the influence of proton concentration on photocatalytic CO_2 reduction. Higher proton concentration significantly increased the H_2 and HCOOH evolution rate in two reaction modes, while the CH_4 and CO evolution was slightly increased in the gas-solid mode (Table S2 in Supporting information), which demonstrates the more efficient facilitation of sufficient protons supply for the conversion of CO_2-to-HCOOH rather than CO_2-to-CO/CH_4. Therefore, above results reveal that suitable reaction mode selection is crucial for the yield and selectivity of the photocatalytic reduction products.

Although the development of CO_2 reduction has attracted much attention in the photocatalytic field, this work firstly focuses on the influence of the reaction modes in the establishment of an efficient catalytic system for photocatalytic reduction of CO_2 in pure water systems. As indicated by the comparison of gas-solid and liquid-solid modes of MOF-involved photocatalysis, the activity and selectivity of CO_2 conversion tend to can be significantly affected by the different reaction systems, between which, the liquid-solid system generates HCOOH with around 100% of selectivity, while gas-solid system contributes to the formation of gas-phase products, such as CO and CH_4. The measurement of *in-situ* FTIRS demonstrated that the different reaction consequence may be attributed to the distinct proton supply capacity, which might have effect on the CO_2 bringing modes. This exploration provides a guidance for the selective control of photocatalytic reduction of CO_2 with H_2O as the reaction solvent.

Declaration of competing interest

The authors declare no conflict of interest.

Acknowledgments

The authors gratefully acknowledge the Fujian Science Technology Innovation Laboratory for Optoelectronic Information of China (Nos. 2021ZR105, 2021ZZ103) and the National Natural Science Foundation of China (Nos. 22071246, 22033008).

Supplementary materials

Supplementary material associated with this article can be found, in the online version, at doi:10.1016/j.cclet.2023.108517.

References

[1] R. Li, W. Zhang, K. Zhou, Adv. Mater. 30 (2018) 1705512.
[2] H.B. Huang, Z.B. Fang, R. Wang, et al., Small 18 (2022) 2200407.
[3] J.H. Zhang, Y.C. Wang, H.J. Wang, D.C. Zhong, T.B. Lu, Chin. Chem. Lett. 33 (2022) 2065–2068.
[4] A.A. Zhang, D.H. Si, H.B. Huang, et al., Angew. Chem. Int. Ed. 61 (2022) 202203955.
[5] L.S. Chen, Q.Q. Tang, S.H. Wu, et al., Chin. Chem. Lett. 34 (2023) 107903.
[6] A.A. Zhang, R. Wang, H.B. Huang, T.F. Liu, R. Cao, Chin. Chem. Lett. 34 (2023) 107311.
[7] P.Y. Kuang, Z.R. Ni, J.G. Yu, J.X. Low, Mater. Rep. Energy 2 (2022) 100081.
[8] S.S. Fu, S. Yao, S. Guo, et al., J. Am. Chem. Soc. 143 (2021) 20792–20801.
[9] Y. Ma, X.L. Wang, Y.S. Jia, et al., Chem. Rev. 114 (2014) 9987–10043.
[10] W.J. Shen, Y.D. Dong, F.Z. Huang, Y.B. Cheng, J. Zhong, Mater. Rep. Energy 1 (2021) 10060.
[11] Q.Q. Huang, Z.B. Fang, K. Pang, et al., Adv. Funct. Mater. 32 (2022) 2205147.
[12] L. Li, Z.B. Fang, W.Z. Deng, et al., CCS Chem. 4 (2022) 2782–2792.
[13] X.J. Hu, Z.X. Li, H. Xue, et al., CCS Chem. 2 (2020) 616–622.
[14] Q.Q. Huang, Y. Hu, Y. Pei, J.H. Zhang, M.L. Fu, Appl. Catal. B 259 (2019) 118106.
[15] L.Y. Chen, Q.L. Liu, J. Yang, Y.L. Li, G.Q. Li, Chin. Chem. Lett. 34 (2023) 107335.
[16] S. Guo, L.H. Kong, P. Wang, et al., Angew. Chem. Int. Ed. 61 (2022) 202206193.
[17] T. Luo, J. Zhang, W. Li, et al., ACS Appl. Mater. Interfaces 9 (2017) 41594–41598.
[18] Z.B. Fang, T.T. Liu, J.X. Liu, et al., J. Am. Chem. Soc. 142 (2020) 12515–12523.
[19] D. Li, M. Kassymova, X. Cai, S.Q. Zang, H.L. Jiang, Coord. Chem. Rev. 412 (2020) 213262.
[20] T.C. Zhuo, Y. Song, G.L. Zhuang, et al., J. Am. Chem. Soc. 143 (2021) 6114–6122.
[21] J.W. Wang, L.Z. Qiao, H.D. Nie, et al., Nat. Commun. 12 (2021) 813.
[22] H.W. Chang, Y.N. Zhou, S.Y. Zhang, X.L. Zheng, Q. Xu, Adv. Mater. Interfaces 8 (2021) 2100205.
[23] Y. Wang, N.Y. Huang, J.Q. Shen, et al., J. Am. Chem. Soc. 140 (2018) 38–41.
[24] Y.H. Fu, D.R. Sun, Y.J. Chen, et al., Angew. Chem. Int. Ed. 51 (2012) 3364–3367.
[25] P. Horcajada, S. Surble, C. Serre, et al., Chem. Commun. 27 (2007) 2820–2822.
[26] X.Y. Dao, J.H. Guo, X.Y. Zhang, et al., J. Mater. Chem. A 8 (2020) 25850–25856.
[27] X.Y. Zhang, P. Wang, Y. Zhang, X.M. Cheng, W.Y. Sun, ACS Appl. Mater. Interfaces 15 (2023) 3348–3356.
[28] J.T. Feaster, C. Shi, E.R. Cave, et al., ACS Catal. 7 (2017) 4822–4827.
[29] S. Kattel, B.H. Yan, Y.X. Yang, J.G. Chen, P. Liu, J. Am. Chem. Soc. 138 (2016) 12440–12450.
[30] M.Y. He, J.M. White, J. Mol. Catal. 30 (1985) 415–430.
[31] T. Yan, P. Wang, W.Y. Sun, Small 19 (2023) 2206070.
[32] F. Guo, R.X. Li, S. Yang, et al., Angew. Chem. Int. Ed. 62 (2023) 202216232.
[33] J.C. Zhu, W.W. Shao, X.D. Li, et al., J. Am. Chem. Soc. 143 (2021) 18233–18241.
[34] Y. Zhang, X.Y. Zhang, W.Y. Sun, ACS Catal. 13 (2023) 1553–15445.
[35] C. Du, X. Wang, W. Chen, et al., Mater. Today Adv. 6 (2020) 100071.
[36] M. Bhattacharya, S. Sebghati, R.T. VanderLinden, C.T. Saouma, J. Am. Chem. Soc. 142 (2020) 17589–17597.
[37] S. Dey, F. Masero, E. Brack, M. Fontecave, V. Mougel, Nature 607 (2022) 499–506.
[38] M.H. Ronne, D. Cho, M.R. Madsen, et al., J. Am. Chem. Soc. 142 (2020) 4265–4275.
[39] N.D. Loewen, E.J. Thompson, M. Kagan, et al., Chem. Sci. 7 (2016) 2728–2735.
[40] E.E. Benson, C.P. Kubiak, A.J. Sathrum, J.M. Smieja, Chem. Soc. Rev. 38 (2009) 89–99.
[41] N.D. Loewen, T.V. Neelakantan, L.A. Berben, Acc. Chem. Res. 50 (2017) 2362–2370.
[42] M.D. Rail, L.A. Berben, J. Am. Chem. Soc. 133 (2011) 18577–18579.
[43] C. Costentin, M. Robert, J.M. Saveant, Chem. Soc. Rev. 42 (2013) 2423–2436.
[44] P. Kang, C. Cheng, Z. Chen, T.J. Meyer, J. Am. Chem. Soc. 134 (2012) 5500–5503.
[45] T.J. Schmeier, G.E. Dobereiner, R.H. Crabtree, N. Hazari, J. Am. Chem. Soc. 133 (2011) 9274–9277.
[46] S.E. Lee, A. Nasirian, Y.E. Kim, et al., J. Am. Chem. Soc. 142 (2020) 19142–19149.